Copy 206
RM L53J21a

NACA RM L53J21a

NACA

RESEARCH MEMORANDUM

COMPARISON OF FREE-FLIGHT MEASUREMENTS OF THE ZERO-LIFT DRAG RISE OF SIX AIRPLANE CONFIGURATIONS AND THEIR EQUIVALENT BODIES OF REVOLUTION AT TRANSONIC SPEEDS

By James Rudyard Hall

Langley Aeronautical Laboratory
Langley Field, Va.

NATIONAL ADVISORY COMMITTEE
FOR AERONAUTICS

WASHINGTON

January 5, 1954

ERRATA NO. 1

NACA RM L53J21a

COMPARISON OF FREE-FLIGHT MEASUREMENTS OF THE ZERO-LIFT DRAG RISE OF SIX AIRPLANE CONFIGURATIONS AND THEIR EQUIVALENT BODIES OF REVOLUTION AT TRANSONIC SPEEDS

By James Rudyard Hall

January 5, 1954

Page 18: Figure 7(b) is in error in the region $0.475 < x/l < 0.712$, wherein the curves should be smoothly faired instead of humped. The correct values of the A/l^2 in this region are tabulated below.

x/l	A/l^2	
	Mass flow ratio = 0	Mass flow ratio = 0.7
0.524	0.0216	0.0200
.562	.0225	.0209
.674	.0221	.0206

NACA-Langley - 2-23-54 - 230

NATIONAL ADVISORY COMMITTEE FOR AERONAUTICS

RESEARCH MEMORANDUM

COMPARISON OF FREE-FLIGHT MEASUREMENTS OF THE ZERO-LIFT DRAG RISE OF SIX AIRPLANE CONFIGURATIONS AND THEIR EQUIVALENT BODIES OF REVOLUTION AT TRANSONIC SPEEDS

By James Rudyard Hall

SUMMARY

Free-flight drag measurements are presented which show the practicability of duplicating the zero-lift drag rise of many airplane configurations by simple bodies of revolution. The results confirm the transonic area rule for straight wings, and for delta and modified-delta wings with and without nacelles. The results showed that the area rule did not apply to one swept-wing configuration and an explanation is advanced to explain why it does not apply.

INTRODUCTION

The recent promulgation of the transonic area rule has produced widespread interest in the practicability of assessing the drag rise of a complete airplane configuration by the use of a simple equivalent body of revolution. In order to investigate the applicability of the area rule for this purpose, the Langley helium gun at the Pilotless Aircraft Research Station, Wallops Island, Va., was used to obtain drag measurements of equivalent bodies of revolution of six configurations having straight wings or swept wings, or having delta or modified-delta wings with and without nacelles. Results are presented and compared with previously obtained rocket-model drag measurements of the complete configurations through a range of Mach numbers varying between 0.8 to 1.3.

SYMBOLS

a	model longitudinal acceleration, ft/sec^2
A	cross-sectional area, sq in.
$\bar{c}$	mean aerodynamic chord, ft
C_D	coefficient of drag, based on S_W
$\Delta C_D = C_D - C_{D_{M=Subsonic}}$	
$\Delta C_{D_{max}}$	maximum ΔC_D
g	acceleration due to gravity, 32.2 ft/sec^2
l	model length, in.
M	Mach number
q	dynamic pressure, lb/sq ft
r	radius of equivalent body of revolution, in.
S_F	maximum cross-sectional area of body of revolution, sq ft
S_W	total wing area, sq ft
t	wing thickness, ft
W	model weight, lb
γ	model flight-path angle, deg

APPARATUS AND METHOD

Photographs of the test models are shown in figure 1. The models were tested by firing them from the Langley helium gun at the Pilotless Aircraft Research Station, Wallops Island, Va. The gun is pictured in figure 2. In operation, a model is placed in a 6-inch-diameter sabot (fig. 3) in the breech of the gun. A push plate behind the sabot bears against it and the model as is shown in the cutaway photograph of the sabot assembly in figure 3. A quick-opening valve admits helium to the

gun barrel under about 200 lb/sq in. pressure, accelerating the sabot assembly down the 23-foot barrel to supersonic velocities. Upon emerging from the barrel, the three segments of the sabot and the push plate peel away, falling to earth within 50 yards and then the model decelerates along a ballistic trajectory during which period a continuous velocity history is obtained by means of the CW Doppler velocimeter.

The model designations are given in table I which also lists pertinent physical dimensions of the bodies of revolution and the corresponding airplane configurations. The models were fin-stabilized bodies of revolution having the same longitudinal distribution of cross-sectional area as the corresponding airplane configurations. This was accomplished by subtracting the fin cross-sectional area from the body area at corresponding stations. The general arrangement of each airplane is given in the (a) parts of figures 4 to 9. The nondimensional radius distribution and area distribution of each airplane is given in the (b) parts of figures 4 to 9.

In order to effect a comparison with rocket models tested, equivalent bodies b and e simulated faired intakes and models a, c, d, and f simulated open intakes. Open intakes were simulated by subtracting from the total nacelle cross-sectional area a constant stream-tube area equal to the intake area times the mass-flow ratio at Mach number 1.0. The applicability of this method for sharp-lipped inlets is substantiated in reference 1. The mass-flow ratios used were either obtained from tests or estimated, and are given in the (b) parts of figures 4 to 9.

The scale of the models was chosen to give a maximum model diameter of approximately 1.5 inches. Construction was of magnesium and aluminum. Lead ballast was added as required to locate the center of gravity forward of 60 percent of the length to the fin-trailing-edge—fuselage intercept. Model dimensions were checked and found to be within ±0.003 inch.

TESTS

The model flight path was obtained by integrating the velocity along a ballistic trajectory. Atmospheric conditions aloft were obtained by radiosonde measurements from an ascending balloon that was released at the time of the tests. The model deceleration was computed from the velocity history and the coefficient of drag was computed from the relationship

$$C_D = -\frac{W}{gqS_W}(a + g \sin \gamma)$$

The drag rise ΔC_D was obtained by subtracting the subsonic level of C_D from the supersonic C_D. The effect of the fins is believed to be within the accuracy of the measurements since the pressure drag of the fins which was initially low was further reduced by suitably indenting the bodies in the region of the fins.

The accuracy of the measurements was within the following limits:

C_D	± 0.001
M	± 0.01

The Reynolds numbers of the tests varied from 3.3×10^6 at Mach number 0.75 to 11×10^6 at Mach number 1.3 and are presented in figure 10 for comparison with the Reynolds numbers of the corresponding rocket-model airplane configurations. All Reynolds numbers are based on the total length of the equivalent bodies of revolution.

RESULTS AND DISCUSSION

The measured drag coefficient C_D and the transonic drag rise, ΔC_D for the test models are presented in the (c) and (d) parts of figures 4 to 9. Drag-coefficient measurements from large-scale rocket-model tests of the airplane configurations are compared with the subject model results in these figures. Summary plots of the foregoing information are presented in figure 11 in the form of "line of agreement" charts of maximum drag rise and drag-rise Mach number for the test models and the corresponding airplanes. The drag-rise Mach number was taken at the point where $\frac{dC_D}{dM} = 0.1$.

The transonic area rule of reference 2 states that the zero-lift drag rise of thin, low-aspect-ratio wing-body combinations is primarily dependent on the axial distribution of cross-sectional area of the configuration and that the drag rise of any such configuration is approximately the same as that of its equivalent body of revolution. The configurations tested herein had aspect ratios varying from 1.9 to 3.5 and average thickness ratios up to 7 percent. It can be seen from figure 11(a) that the agreement between the results for the rocket models and corresponding bodies of revolution is within 15 percent in every case except for model b, the swept-wing configuration. Although the swept wing had the highest aspect ratio tested, its equivalent body of revolution has a smooth contour which conforms to the requirements of the area rule. Poor agreement for swept-wing configurations was also reported in references 2 and 3 which indicate a limitation to this application of the transonic area rule.

Recent studies and observations of the flow over wing-body combinations offer a possible explanation of why the ΔC_D of the swept wings cannot be duplicated as well as for other plan forms: The local Mach number over the wing becomes supersonic before the airplane attains supersonic speed, creating a supersonic pressure field along the wing span which interferes with the flow over the fuselage at the wing root. In the case of the swept wing, the interaction of the wing and fuselage pressure fields is concentrated at the root section whereas on the equivalent body of revolution the wing cross-sectional area is distributed over a greater length. This may lead to a lower drag rise for the equivalent body of revolution than for the swept-wing configuration. The effect is not powerful for straight-winged and delta-winged configurations because the zone of pressure interaction and the location of the incremental area due to wing cross-sectional area are more nearly coincident. It is possible that a method of area distribution for swept-wing configurations which locates most of the wing cross-sectional area in the region of the wing root would more nearly simulate the pressure conditions around the airplane and lead to better drag-rise agreement between the equivalent body of revolution and the configuration.

In all cases for which the technique was suitable, except model f, the ΔC_D of the equivalent body was 10 to 15 percent less than the configuration ΔC_D. The values of ΔC_D of model f and configuration f agreed very well, possibly because their area distribution was very favorable and minimized interference effects present in the other configurations.

The presence of nacelles (or stores) does not appear to affect the applicability of the technique since agreement was obtained for a model without nacelles (model c), a model with 2 large nacelles (model e) and a model with 4 nacelles (model f).

The drag rise of the bodies of revolution occurred at a Mach number 0.01 to 0.03 higher than that of the configurations in all cases except for model a, as shown in figure 11(b).

CONCLUDING REMARKS

The free-flight drag measurements reported herein indicate that the transonic drag rise of several straight-, delta-, or modified-delta-winged configurations was duplicated within 15 percent by the drag rise of simple bodies of revolution having the same longitudinal distributions of area as the airplane configurations. The presence of nacelles (or stores) on the delta wing did not affect the applicability of the

technique. The drag rise of the swept-wing configuration did not agree with the drag rise of its equivalent body of revolution and more investigation of this class of wing is needed.

Langley Aeronautical Laboratory,
National Advisory Committee for Aeronautics,
Langley Field, Va., October 6, 1953.

REFERENCES

1. Walters, Richard E.: Application of Transonic Area Rule to a Sharp-Lipped Ducted Nacelle. NACA RM L53J09b, 1953.

2. Whitcomb, Richard T.: A Study of the Zero-Lift Drag-Rise Characteristics of Wing-Body Combinations Near the Speed of Sound. NACA RM L52H08, 1952.

3. Hoffman, Sherwood: An Investigation of the Transonic Area Rule by Flight Tests of a Sweptback Wing on a Cylindrical Body With and Without Body Indentation Between Mach Numbers 0.9 to 1.8. NACA RM L53J20a, 1953.

TABLE I.- PERTINENT PHYSICAL DIMENSIONS OF BODIES OF REVOLUTION AND CORRESPONDING AIRPLANE CONFIGURATIONS

Model	Figure	Wing	Aspect ratio	Average t/c	Nacelles	S_W/S_F	Fineness ratio of equivalent body
a	4	Straight	3.0	0.045	0	5.6	10.0
b	5	Swept	3.5	.07	0	10.0	7.2
c	6	Modified delta	2.0	.029	0	14.0	7.2
d	7	Modified delta	2.0	.055	0	13.4	6.2
e	8	Delta	1.9	.04	2	12.2	6.7
f	9	Modified delta	2.1	.03	4	18.2	9.1

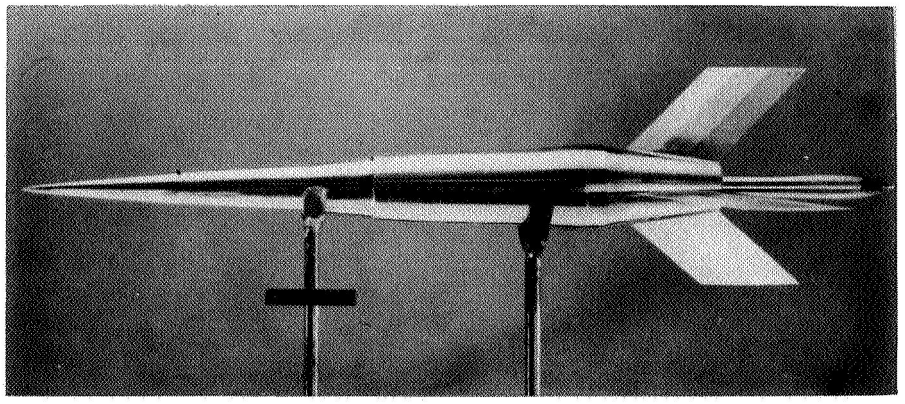

(a) Model a.

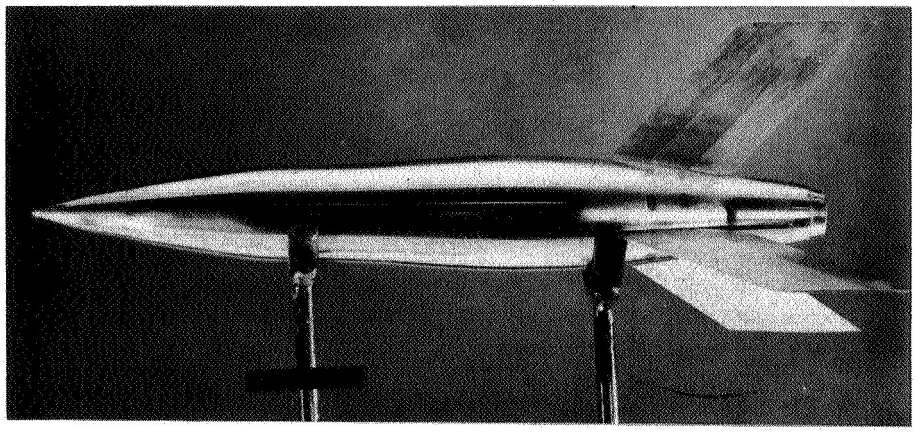

(b) Model b.

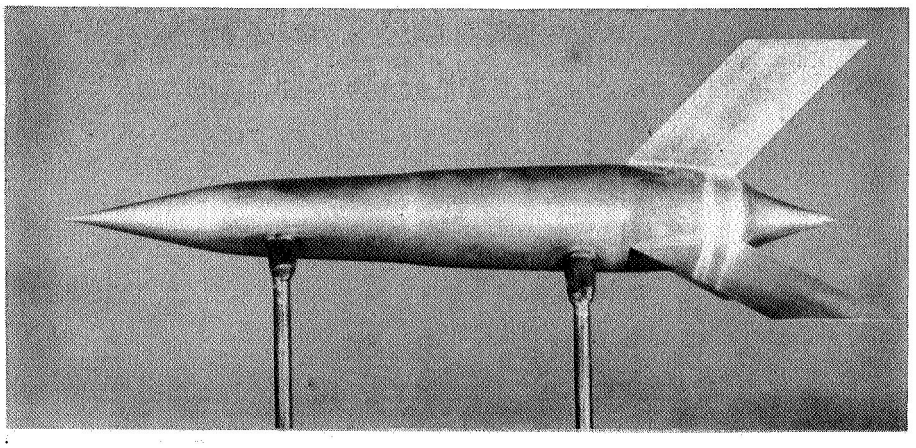

L-81258

(c) Model c.

Figure 1.- Test models.

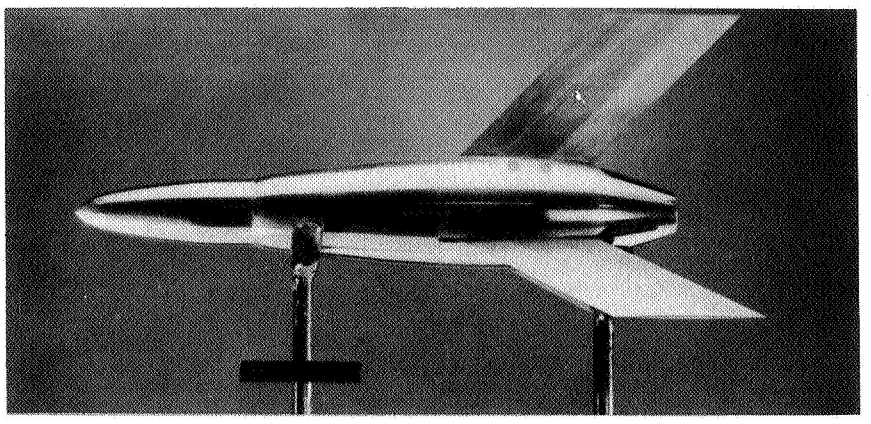

(d) Model d.

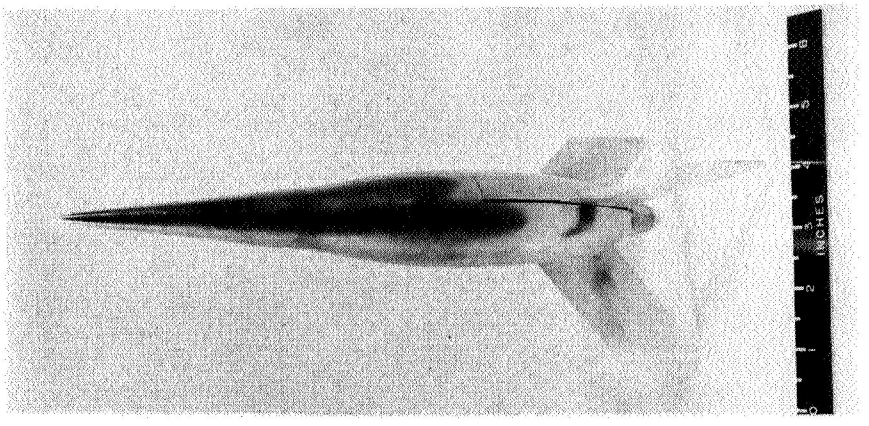

(e) Model e.

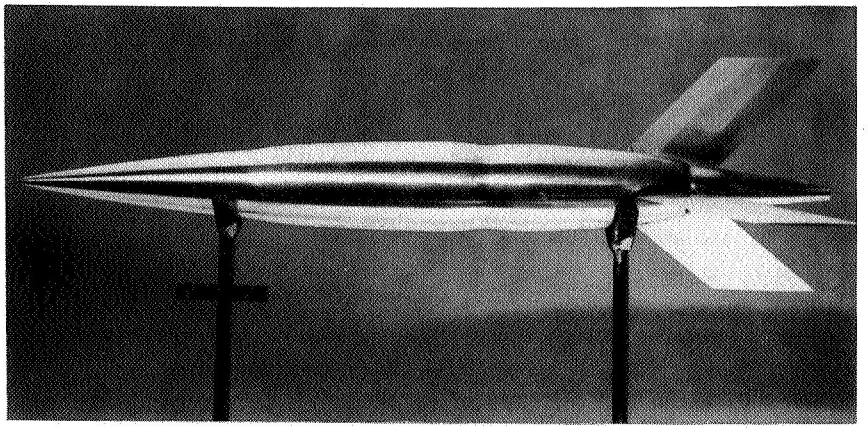

L-81259

(f) Model f.

Figure 1.- Concluded.

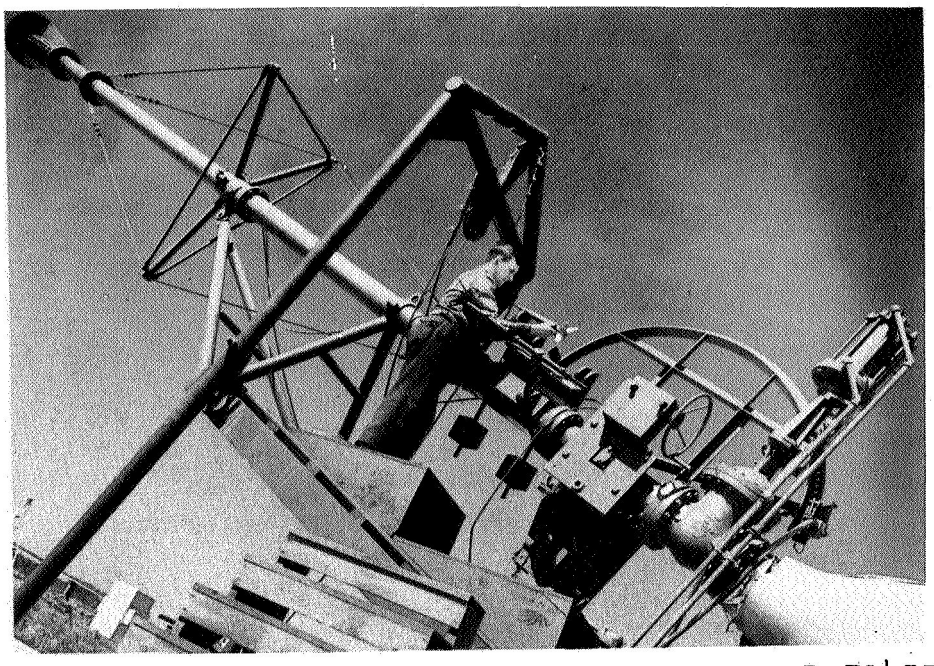

L-71457

(a) Model being placed in helium gun.

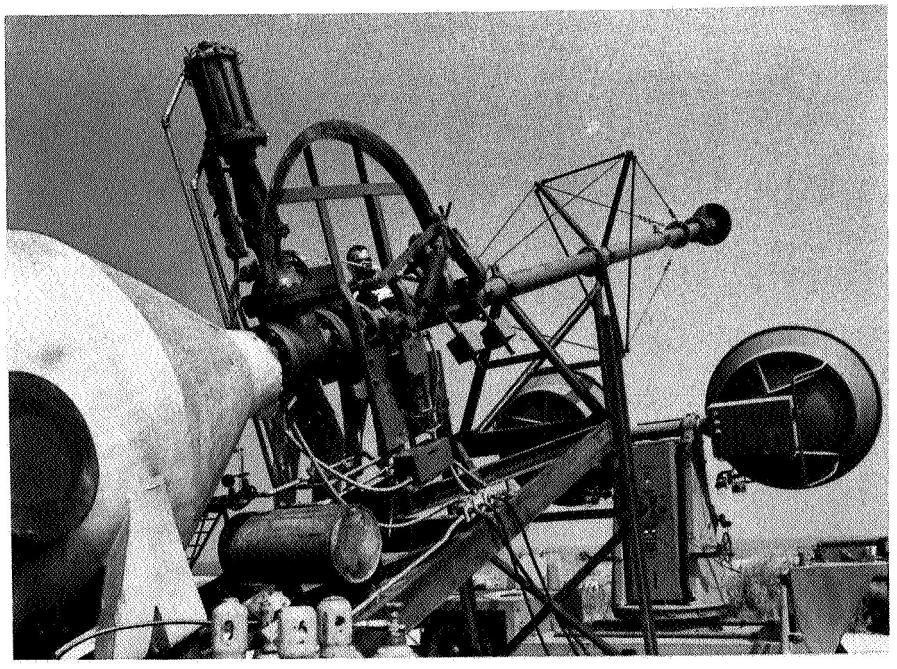

L-66870

(b) General arrangement showing helium supply tank, quick-opening-valve mechanism, barrel and barrel truss, and CW Doppler velocimeter used to track model.

Figure 2.- Helium gun.

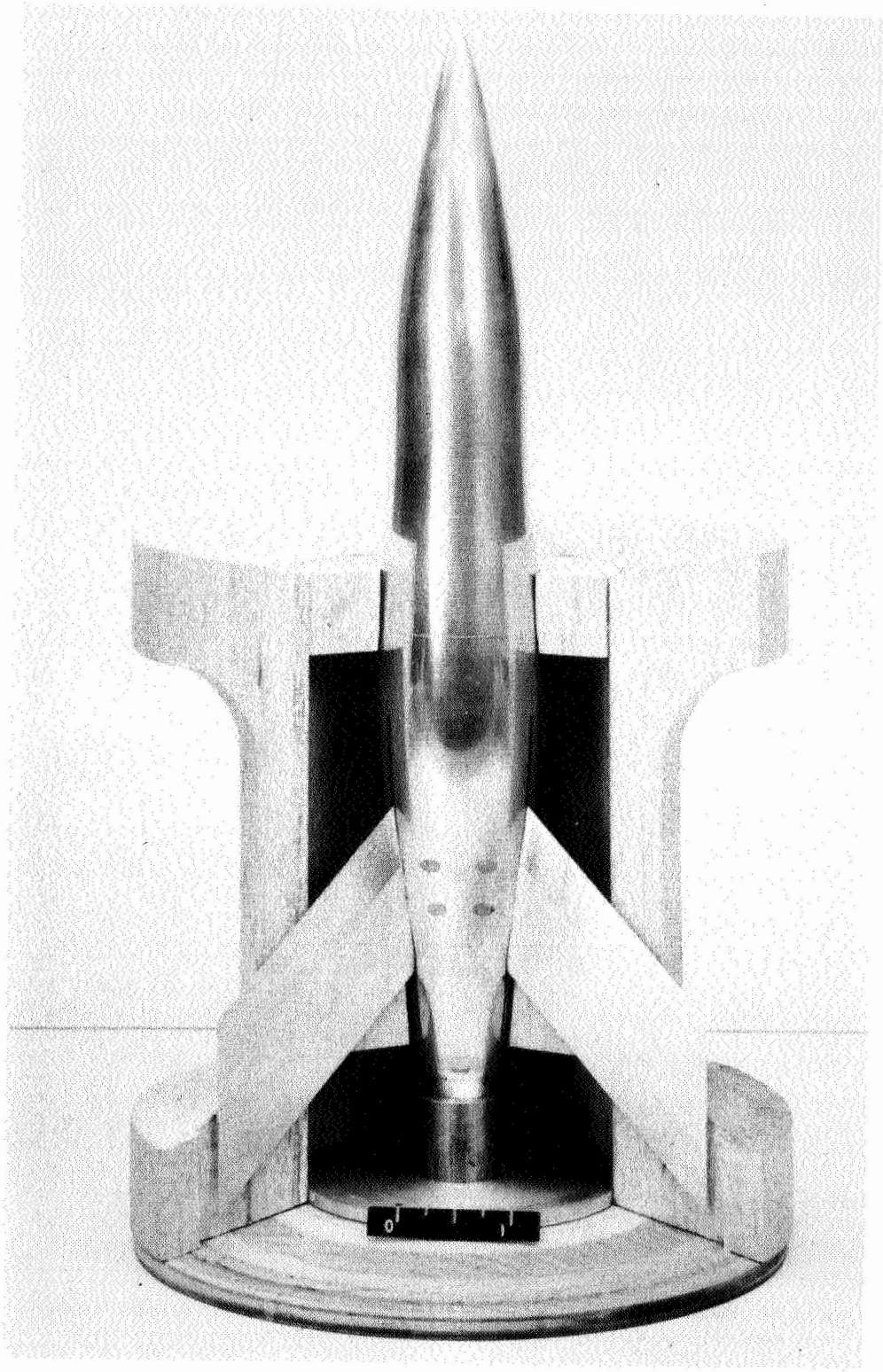

L-79811

Figure 3.- Cutaway photograph of typical model mounted in sabot.

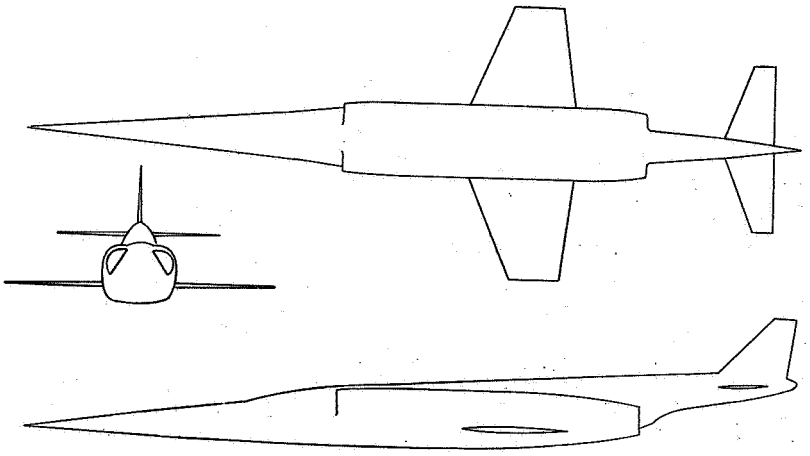

(a) General arrangement of configuration a.

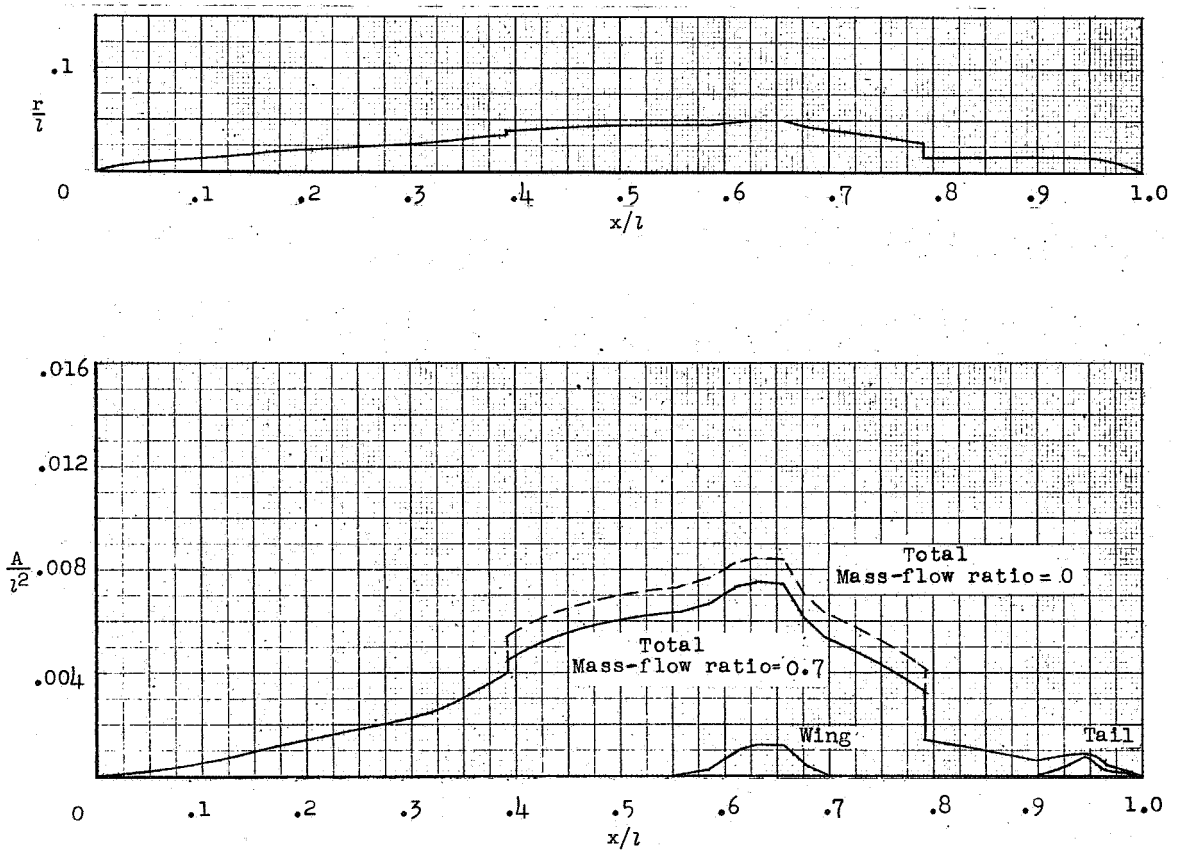

(b) Longitudinal distribution of cross-sectional area and equivalent-body radius.

Figure 4.- Physical characteristics of rocket-model-configuration a and comparison of rocket-model and equivalent-body test results.

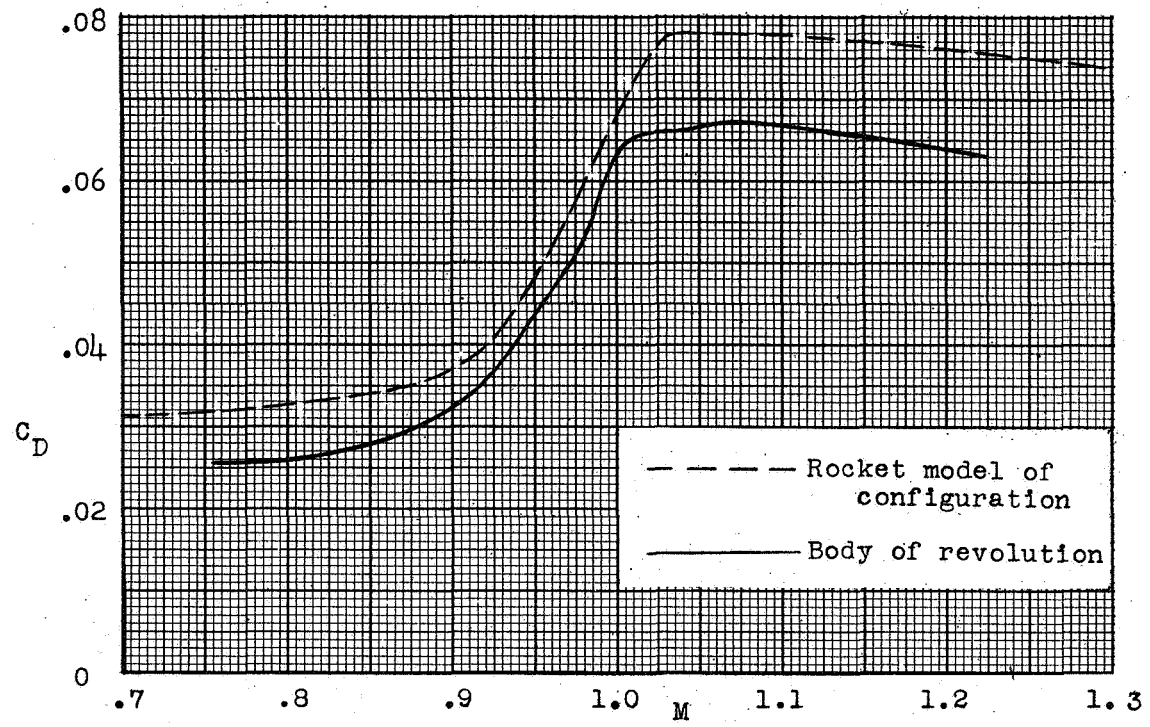

(c) Total C_D based on rocket-model wing area.

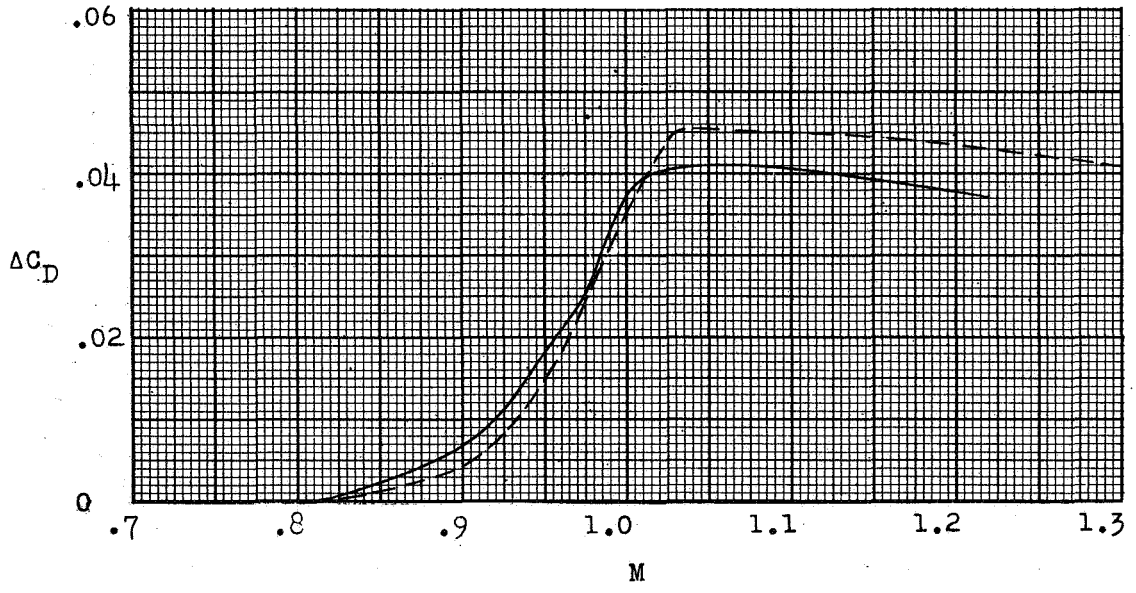

(d) Drag-rise coefficient.

Figure 4.- Concluded.

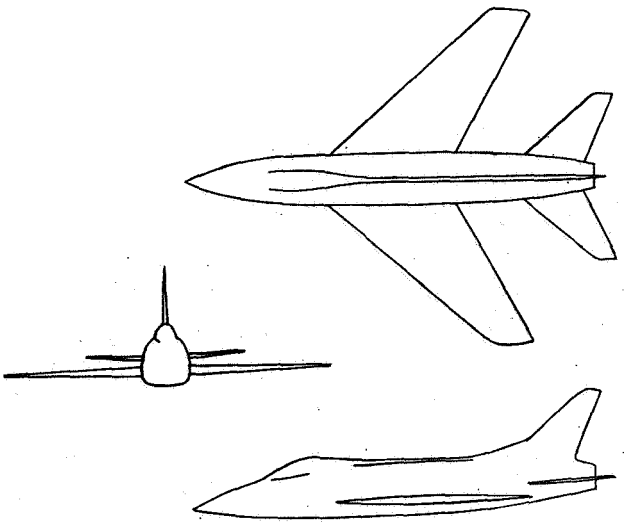

(a) General arrangement of configuration b.

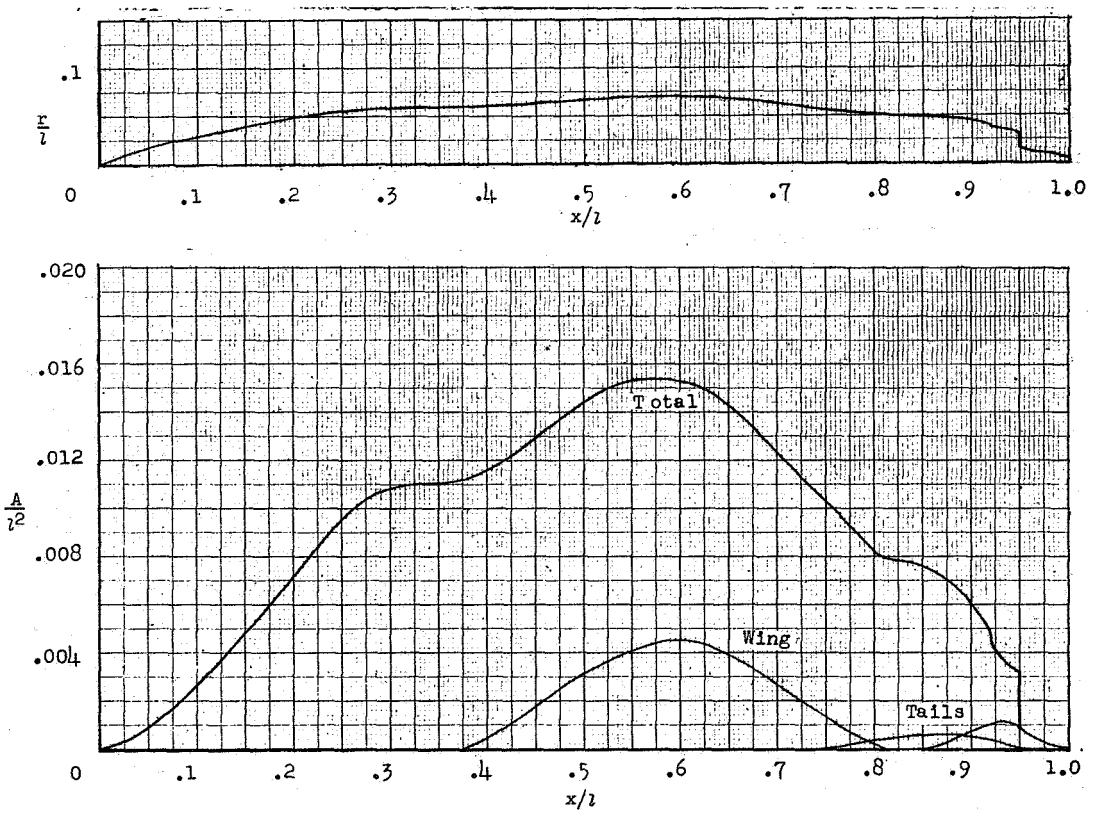

(b) Longitudinal distribution of cross-sectional area and equivalent-body radius.

Figure 5.- Physical characteristics of rocket-model-configuration b and comparison of rocket-model and equivalent-body test results.

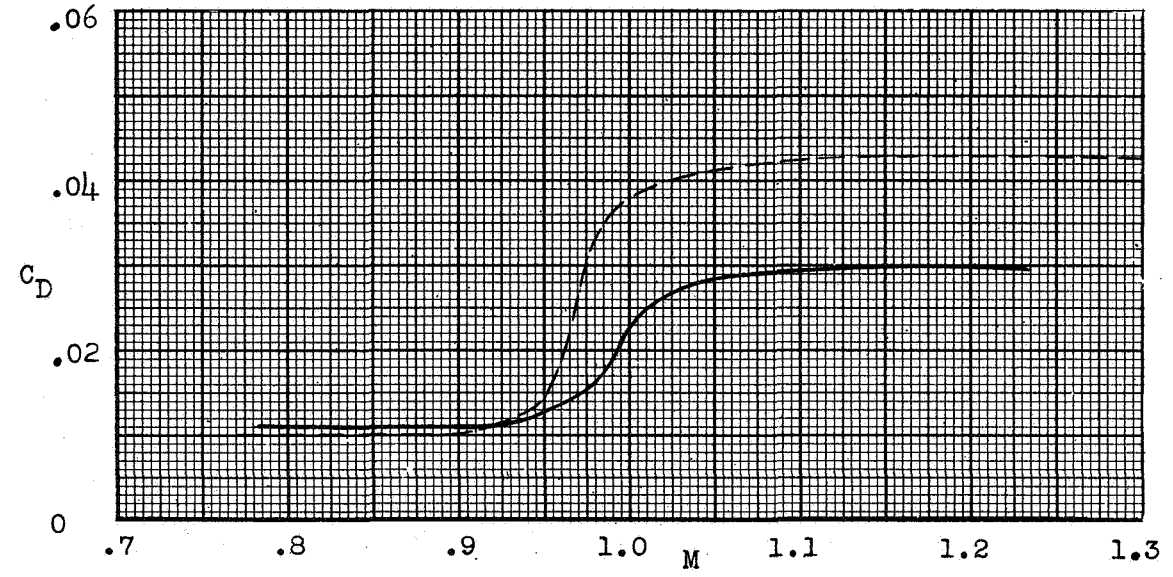

(c) Total C_D based on rocket-model wing area.

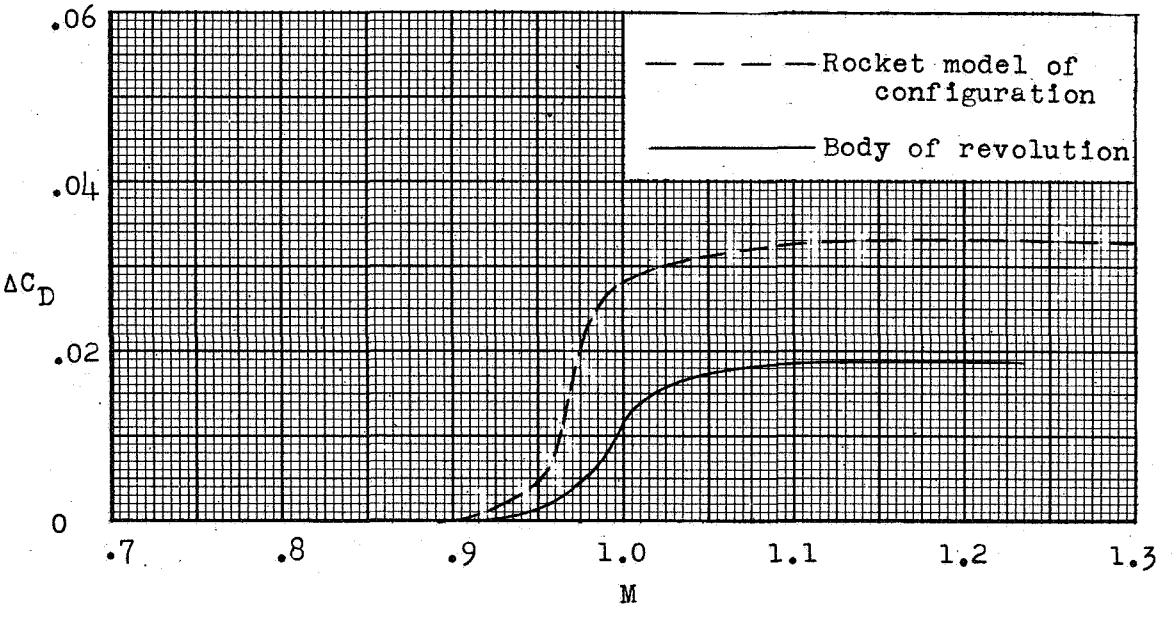

(d) Drag-rise coefficient.

Figure 5.- Concluded.

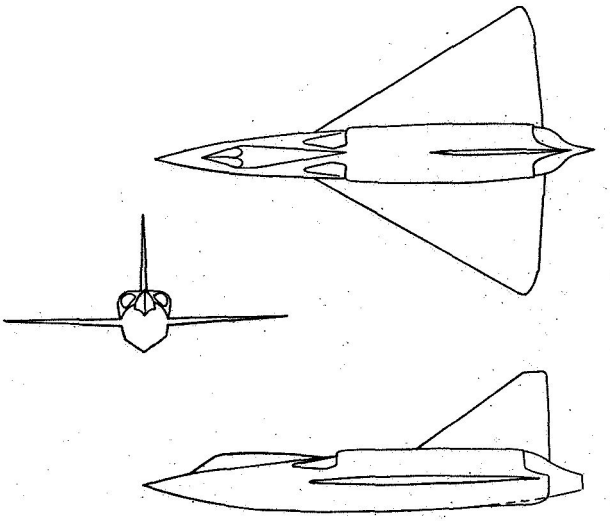

(a) General arrangement of configuration c.

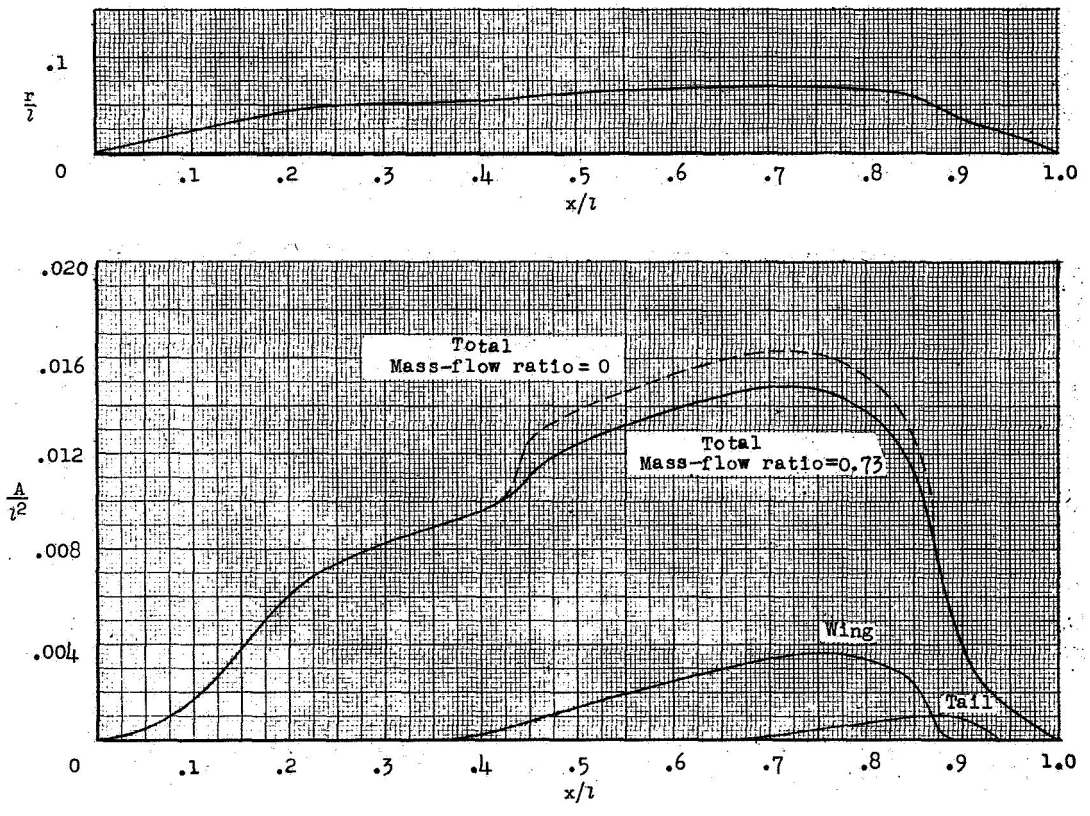

(b) Longitudinal distribution of cross-sectional area and equivalent-body radius.

Figure 6.- Physical characteristics of rocket-model-configuration c and comparison of rocket-model and equivalent-body test results.

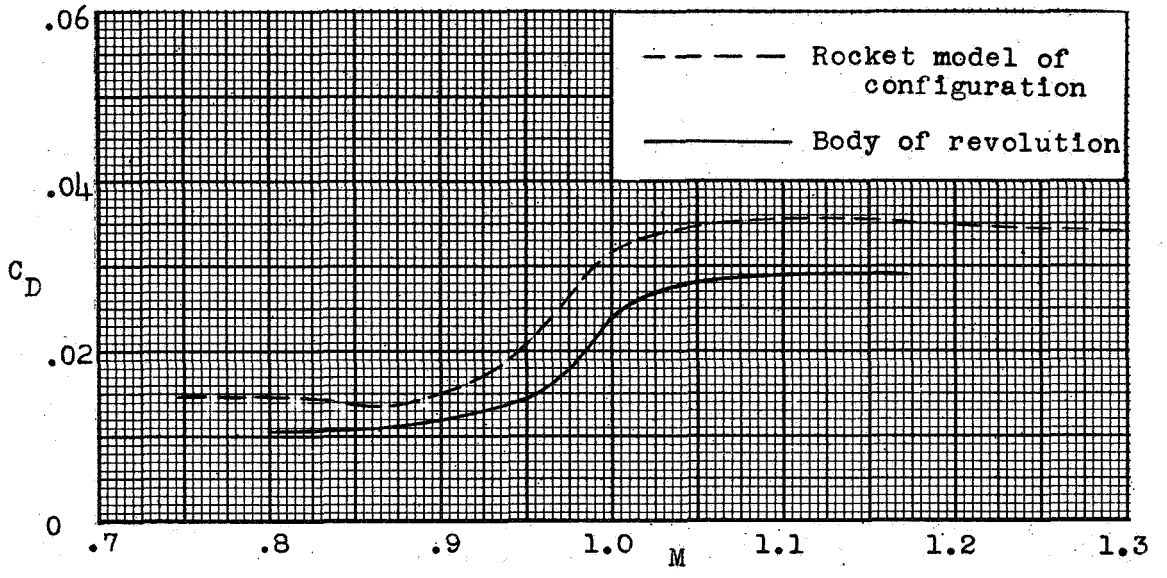

(c) Total C_D based on rocket-model wing area.

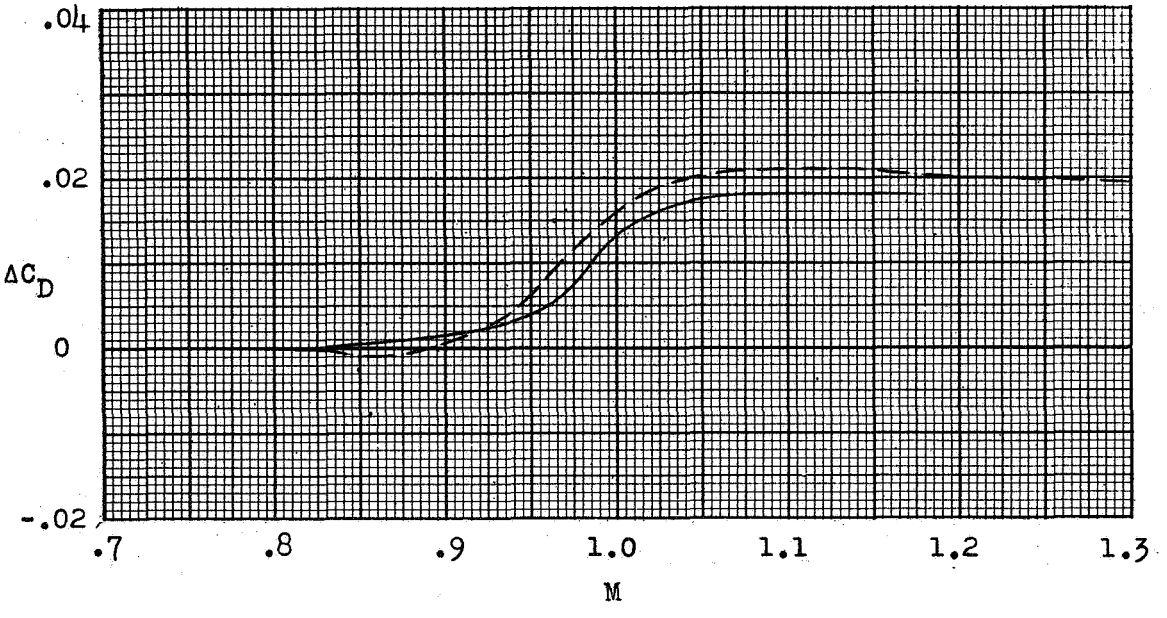

(d) Drag-rise coefficient.

Figure 6.- Concluded.

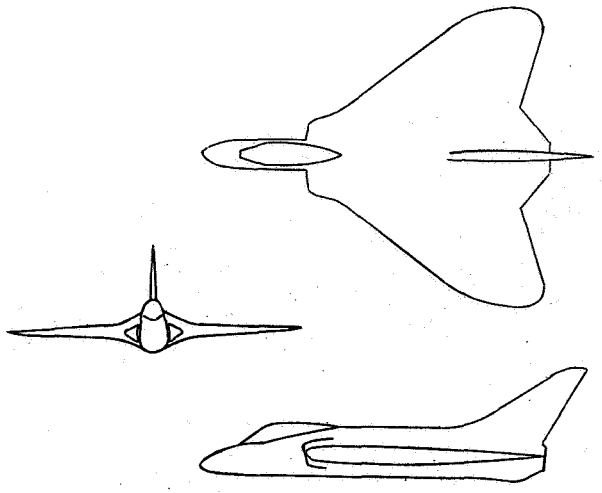

(a) General arrangement of configuration d.

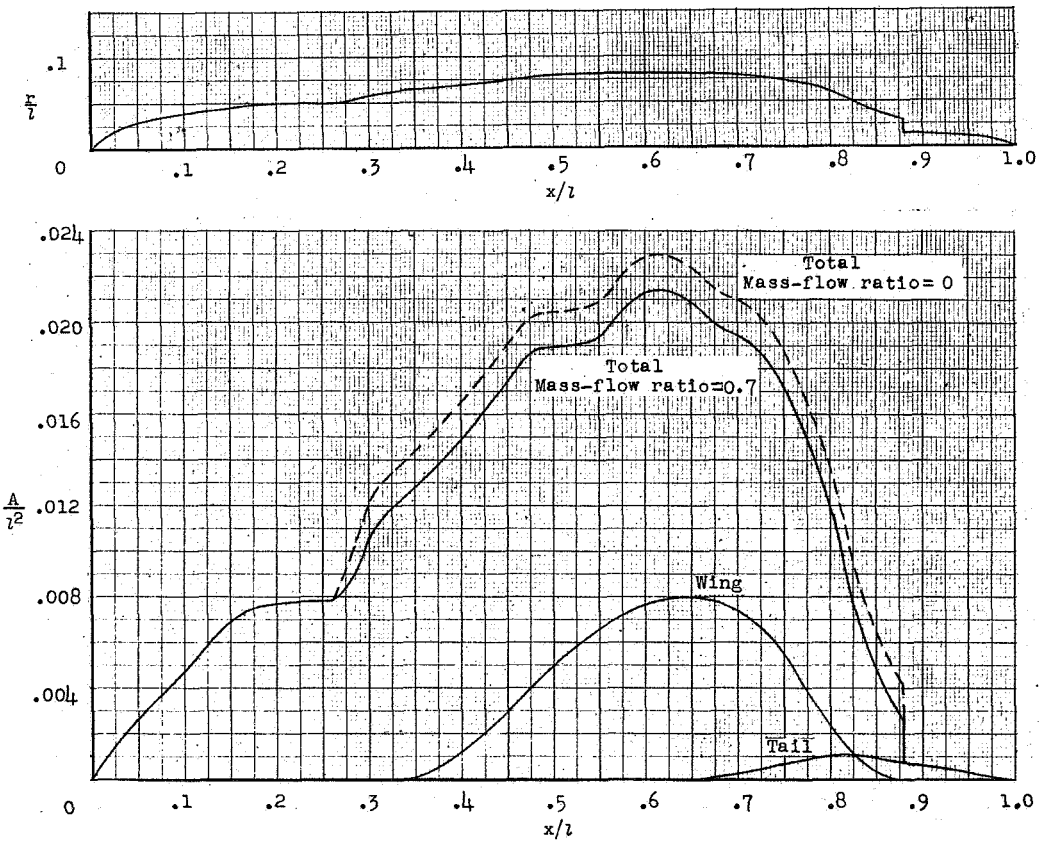

(b) Longitudinal distribution of cross-sectional area and equivalent-body radius.

Figure 7.- Physical characteristics of rocket-model-configuration d and comparison of rocket-model and equivalent-body test results.

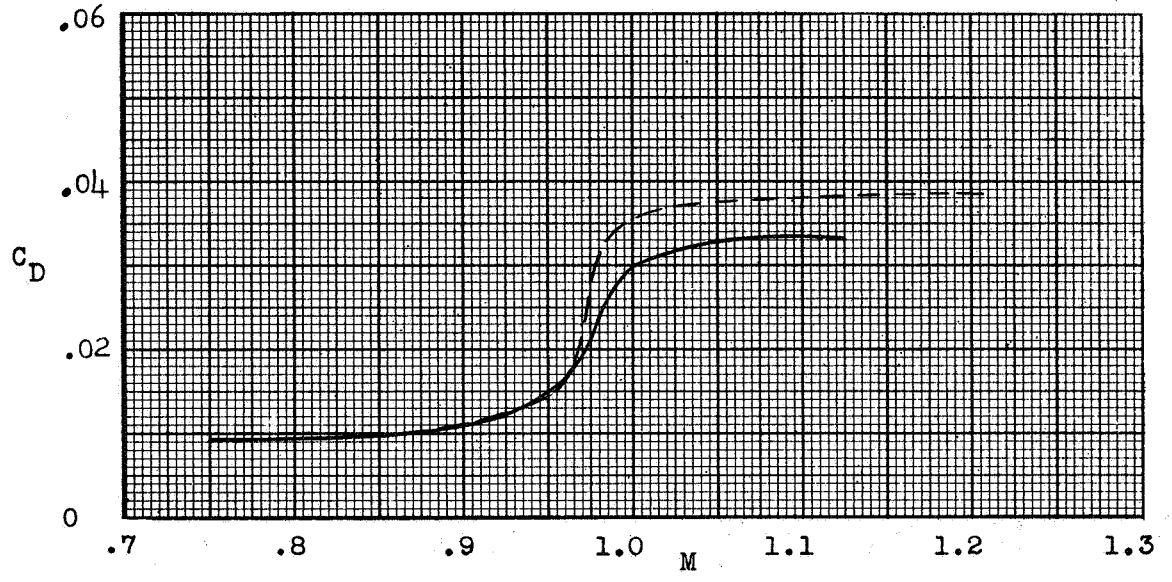

(c) Total C_D based on rocket-model wing area.

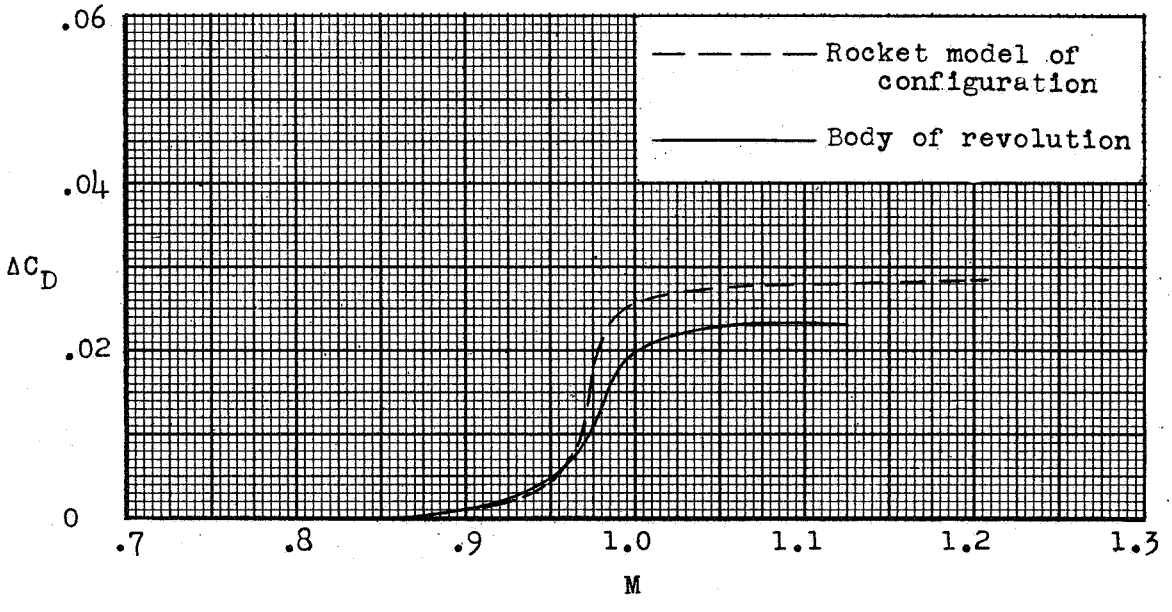

(d) Drag-rise coefficient.

Figure 7.- Concluded.

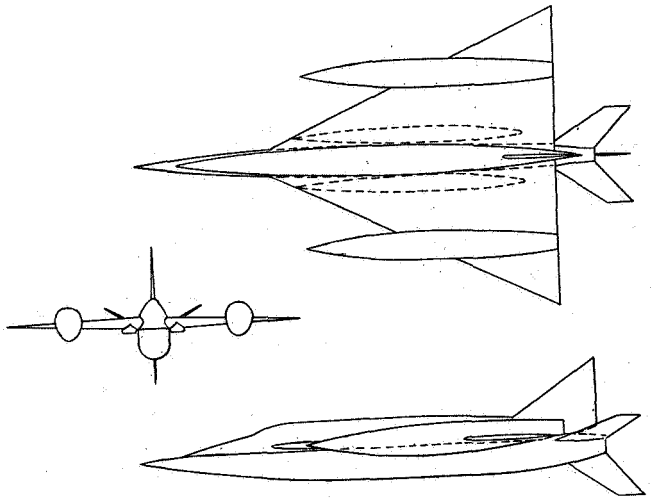

(a) General arrangement of configuration e.

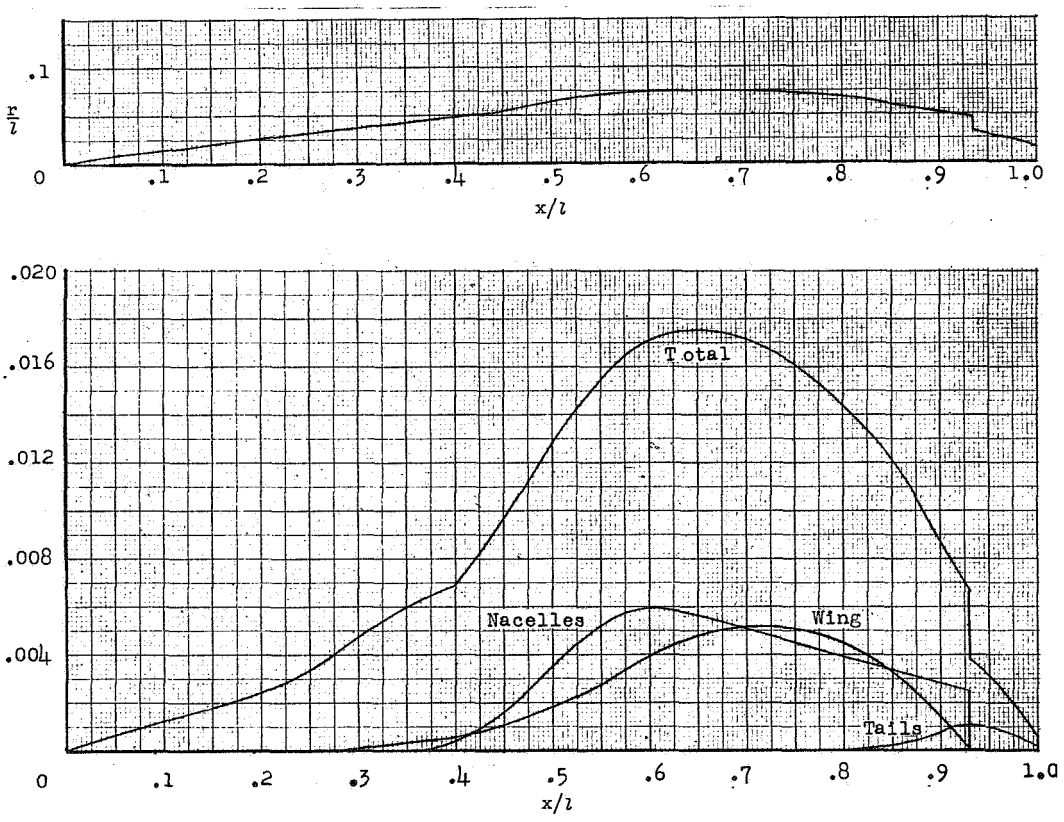

(b) Longitudinal distribution of cross-sectional area and equivalent-body radius.

Figure 8.- Physical characteristics of rocket-model-configuration e and comparison of rocket-model and equivalent-body test results.

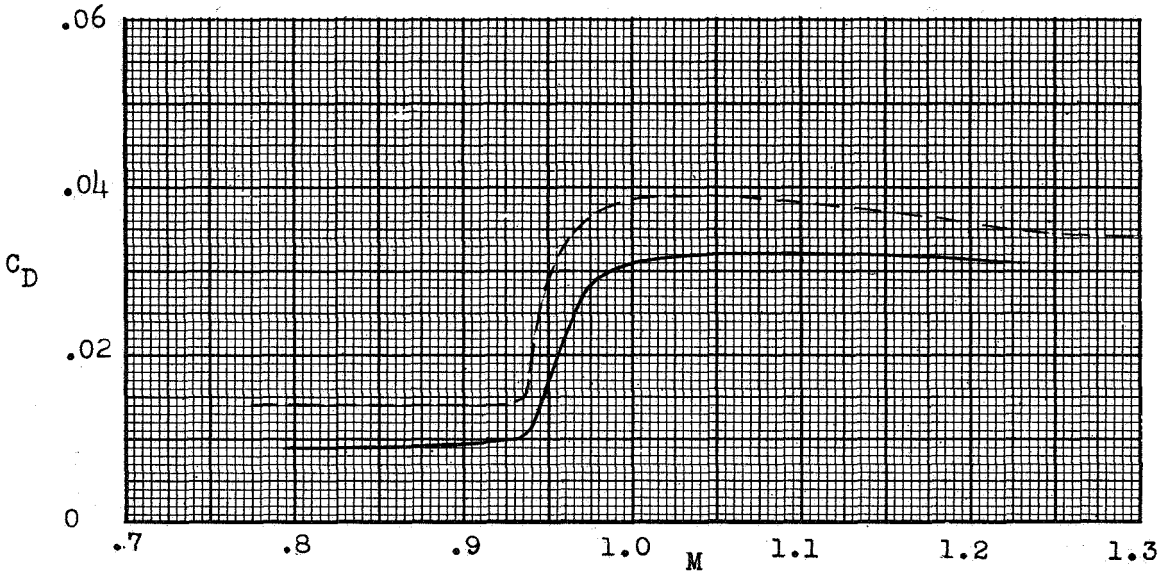

(c) Total C_D based on rocket-model wing area.

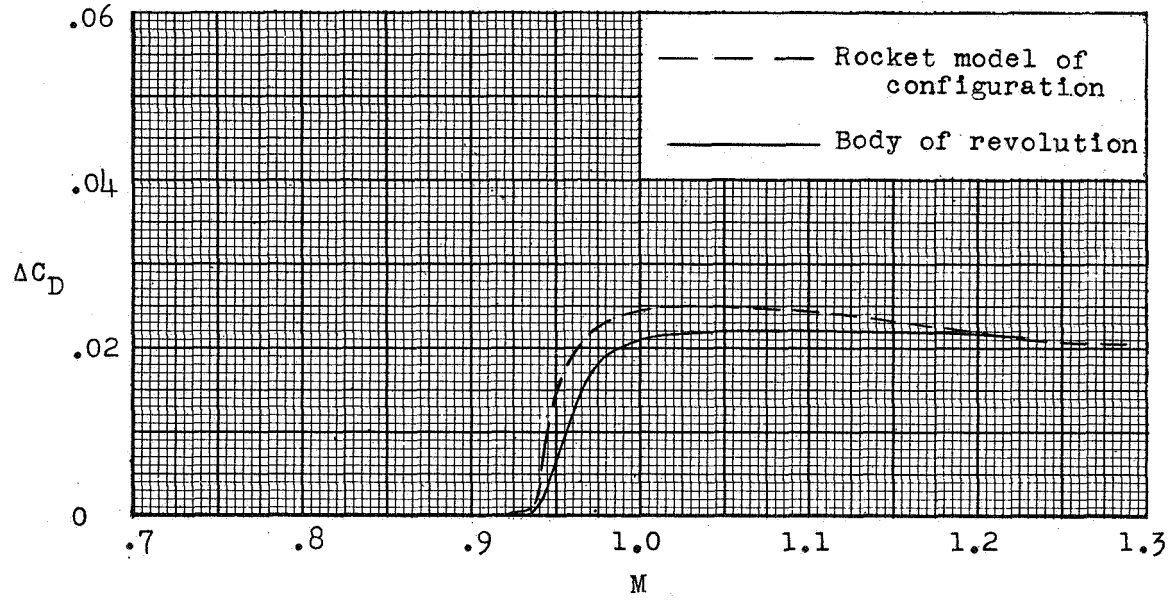

(d) Drag-rise coefficient.

Figure 8.- Concluded.

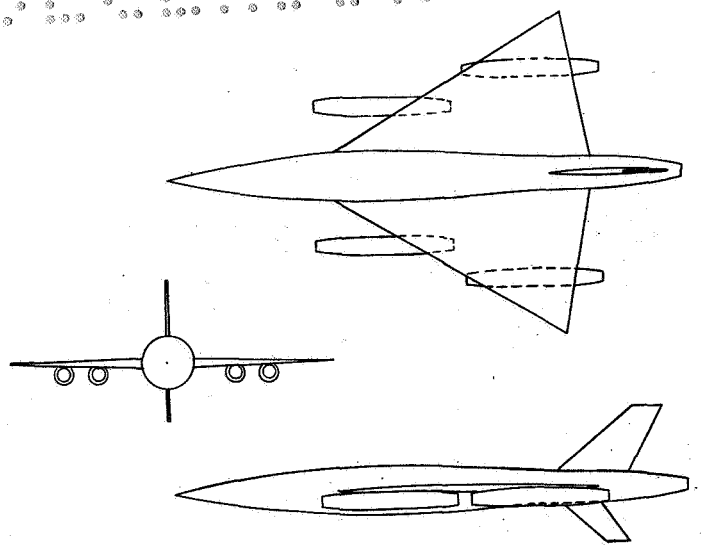

(a) General arrangement of configuration f.

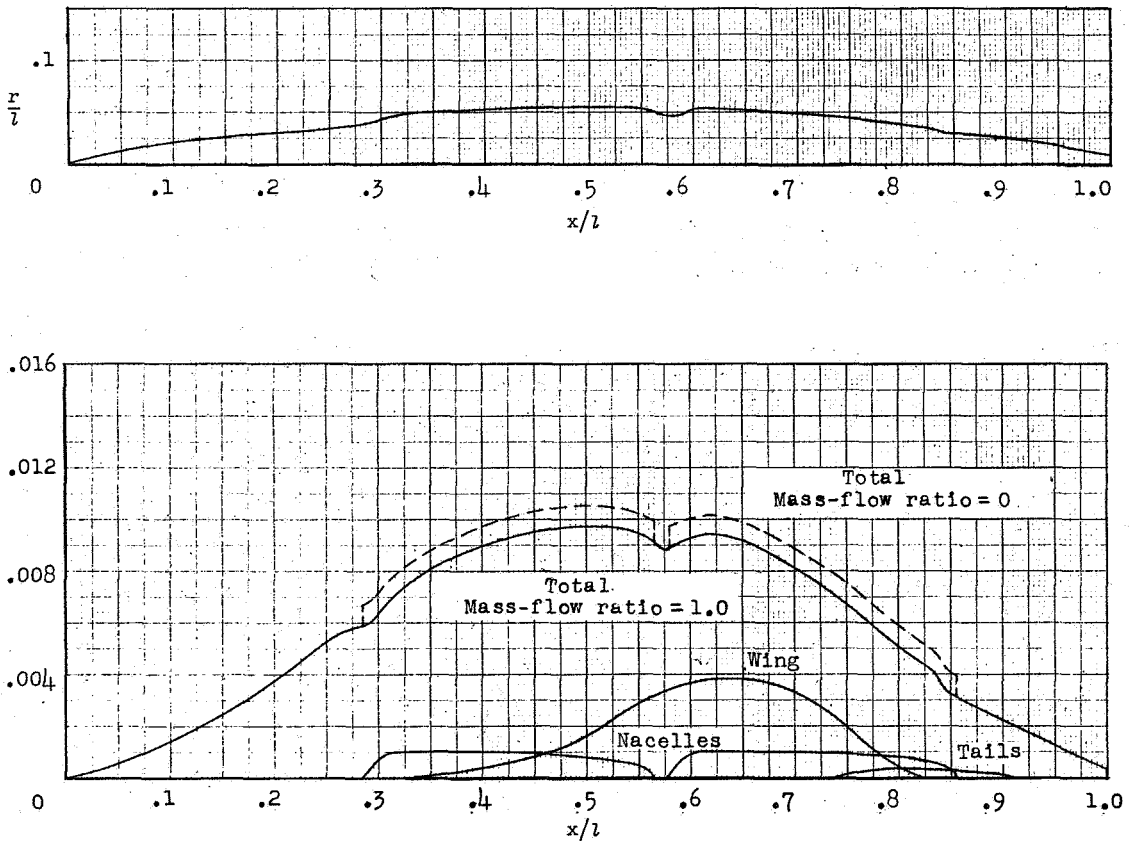

(b) Longitudinal distribution of cross-sectional area and equivalent-body radius.

Figure 9.- Physical characteristics of rocket-model-configuration f and comparison of rocket-model and equivalent-body test results.

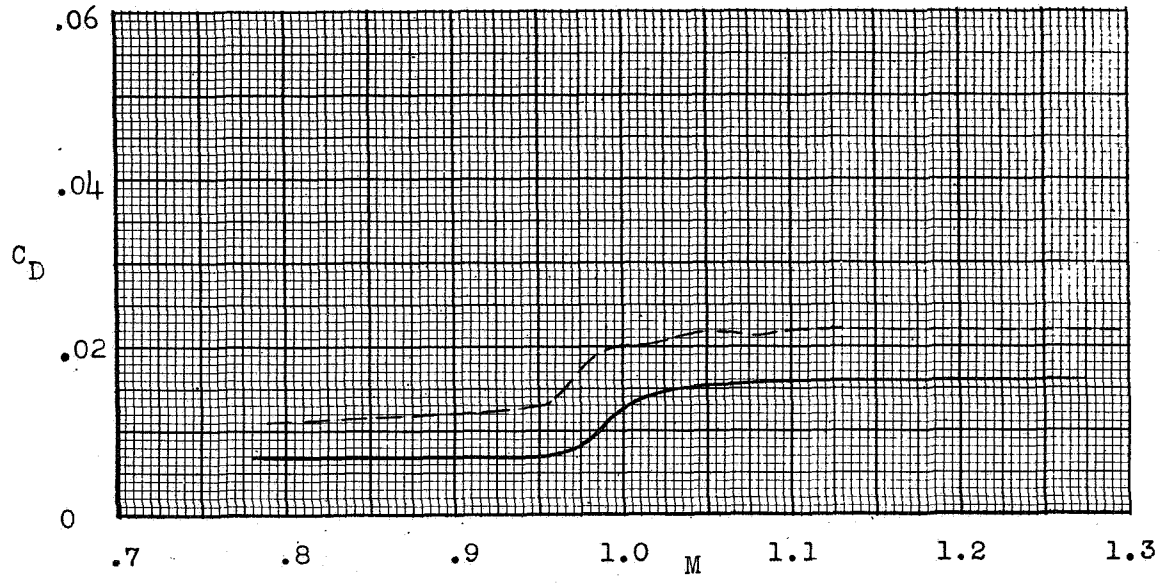

(c) Total C_D based on rocket-model wing area.

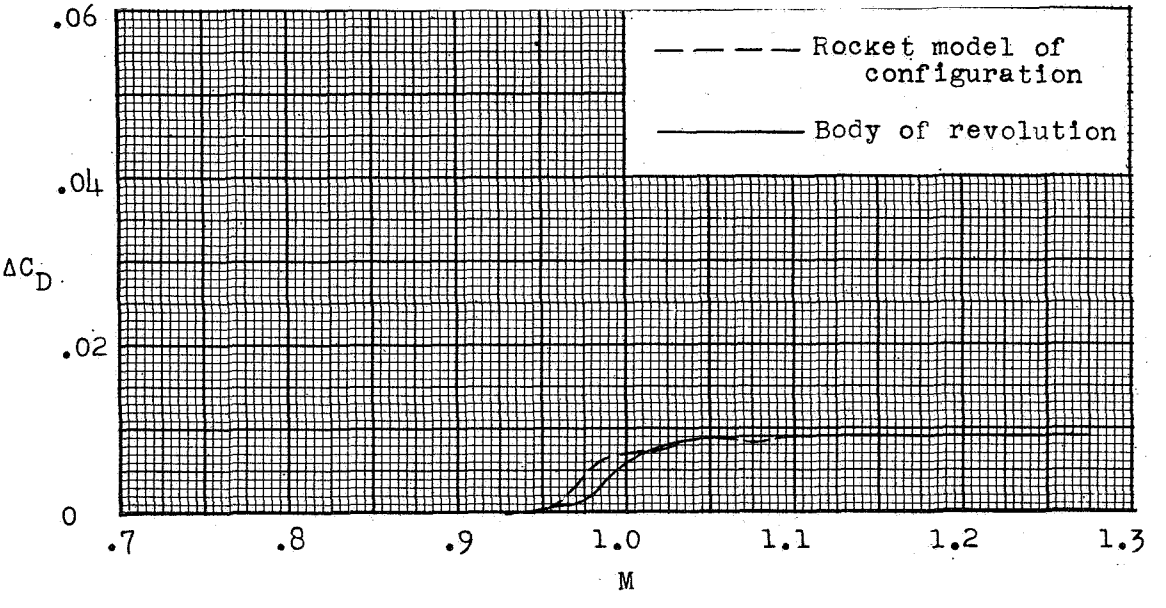

(d) Drag-rise coefficient.

Figure 9.- Concluded.

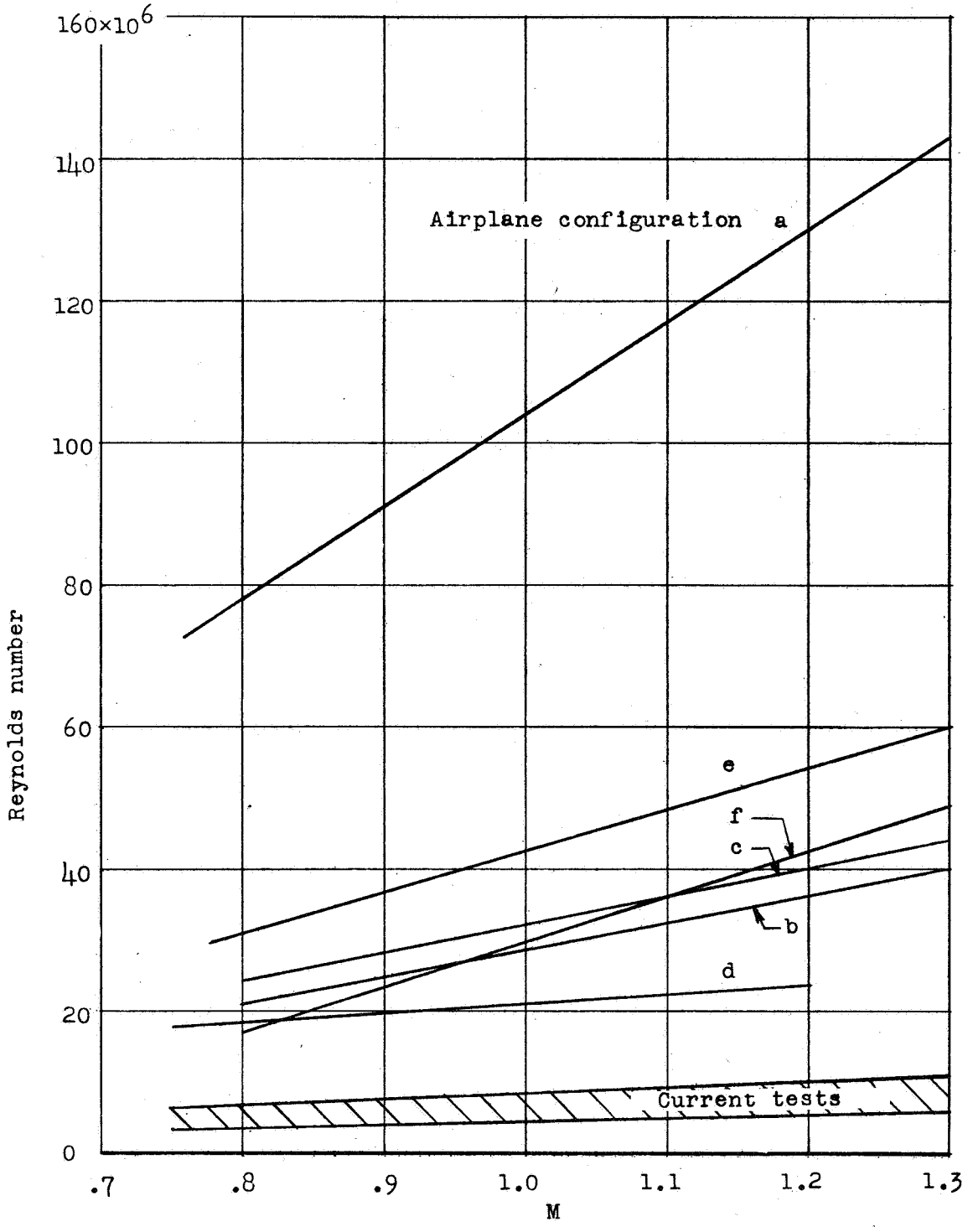

Figure 10.- Reynolds number range of current tests and of rocket-model tests on comparative airplane configurations. Reynolds number is based on length of each model tested.

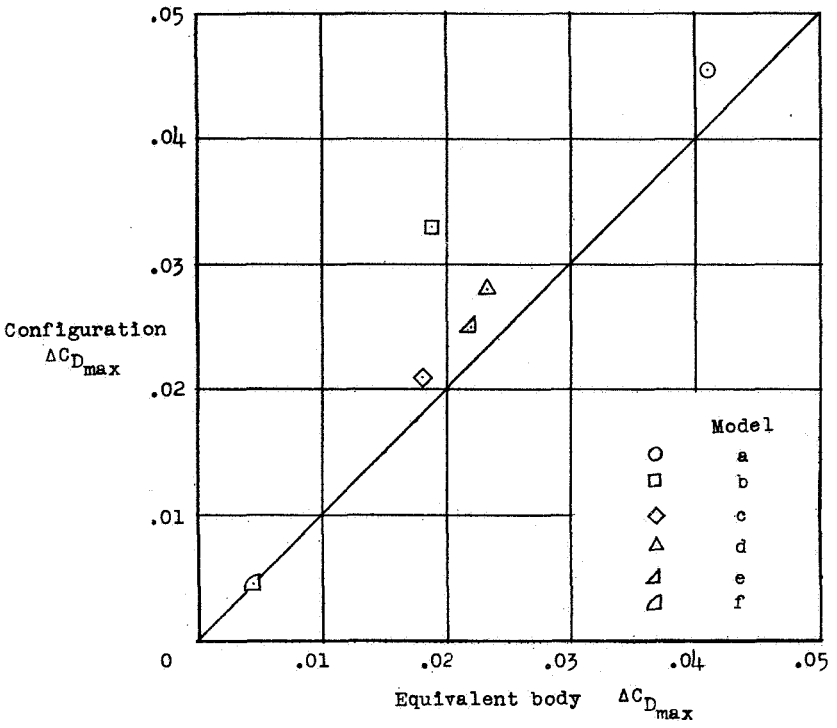

(a) Comparative maximum drag-rise coefficient.

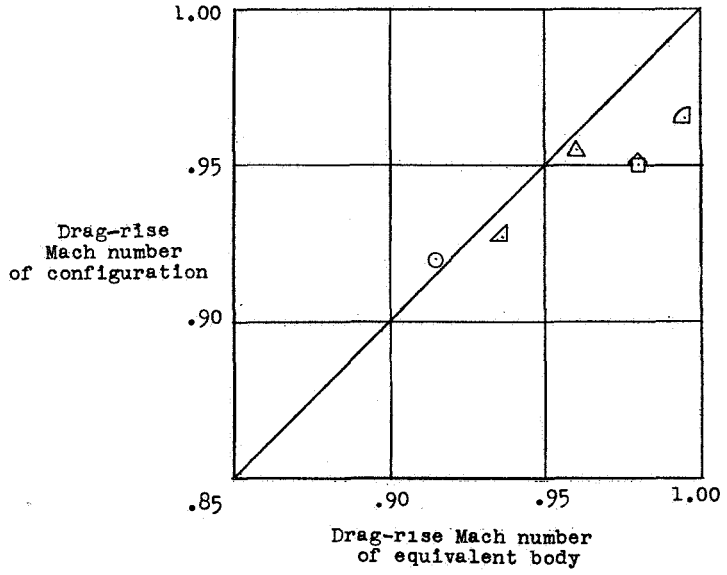

(b) Comparative drag-rise Mach number.

Figure 11.- Agreement of maximum drag-rise coefficient and drag-rise Mach number of currently tested bodies of revolution and the configurations from which they were derived.

NACA-Langley - 1-5-54 - 325